

Verification of Onsager reciprocal relation between anomalous transverse coefficients of an anisotropic antiferromagnet

Xiaodong Guo¹, Xiaokang Li¹, Zengwei Zhu^{1,*} and Kamran Behnia^{2,*}

¹Wuhan National High Magnetic Field Center and School of Physics,
Huazhong University of Science and Technology,
Wuhan, 430074, China

²Laboratoire de Physique et Etude des Matériaux (CNRS/UPMC),
Ecole Supérieure de Physique et de Chimie Industrielles,
10 Rue Vauquelin, 75005 Paris, France

(Dated: July 12, 2023)

Whenever two irreversible processes occur simultaneously, time-reversal symmetry of microscopic dynamics gives rise, on a macroscopic level, to Onsager's reciprocal relations, which impose constraints on the number of independent components of any transport coefficient tensor. Here, we show that in the antiferromagnetic YbMnBi₂, which displays a strong temperature-dependent anisotropy, the Onsager's reciprocal relations are strictly satisfied for anomalous electric, σ_{ij}^A , and anomalous thermoelectric, α_{ij}^A , conductivity tensors. In contradiction with what was recently reported by Pan *et al.* [1], we find that $\sigma_{ij}^A(H) = \sigma_{ji}^A(-H)$, and $\alpha_{ij}^A(H) = \alpha_{ji}^A(-H)$. This equality holds in the whole temperature window irrespective of the relative weights of the intrinsic or extrinsic mechanisms. The $\alpha_{ij}^A/\sigma_{ij}^A$ ratio is close k_B/e at room temperature, but peaks to an unprecedented magnitude of $2.9 k_B/e$ at ~ 150 K, which may involve non-degenerate carriers of small Fermi surface pockets.

Onsager's reciprocal relations are derived by assuming that all microscopic processes are reversible: the future is symmetric to the past [2–8]. This is called time-reversal symmetry. Given a system brought out of equilibrium by the thermodynamic forces F_k , the corresponding fluxes J_i are that, in the coupled transport equation $J_i = \sum_k L_{ik} F_k$, the kinetic coefficients L_{ik} obey the relation $L_{ik} = -L_{ki}$. When the time-reversal symmetry is broken, i.e. applied a magnetic field H . This relation states that the kinetic coefficients obey $L_{ik}(H) = L_{ki}(-H)$. This relation, a cornerstone of nonequilibrium statistical physics, is relevant to any case of two irreversible processes occurring simultaneously.

YbMnBi₂ crystallizes in a $P4/nmm$ structure, as shown in Fig.1(a)[1, 9, 10]. In ordered state, the spin of Mn align antiferromagnetically along the z -axis, but with a canted angle that results in a ferromagnetic component in the xy plane [1, 10–12]. This canted ferromagnetic component lifts the degeneracy of Dirac points and creates Weyl points near the Fermi level [1, 11]. Both anomalous Hall (AHE) and anomalous Nernst (ANE) effects were observed in this system [1]. The maximum Nernst thermopower was found to be remarkably large ($\sim 6 \mu\text{VK}^{-1}$ at 160 K), exceeding the Nernst signal observed in other topological antiferromagnets, such as Mn₃Sn [13–15] ($\sim 0.5 \mu\text{VK}^{-1}$), in Mn₃Ge [14, 16, 17] ($\sim 1.2 \mu\text{VK}^{-1}$).

However, Pan *et al.* [1] report an intriguing breakdown of Onsager's reciprocal relations in both Hall and Nernst conductivities. According to their data (Fig. 4 in ref. [1]), $\sigma_{bc} \neq \sigma_{cb}$ and $\alpha_{bc} \neq \alpha_{cb}$ in YbMnBi₂, over a wide temperature range. This is surprising, because in contrast to the Wiedemann-Franz (WF) law, these relations are a cornerstone of irreversible thermodynamics. It has been checked experimentally [18] that even when the WF

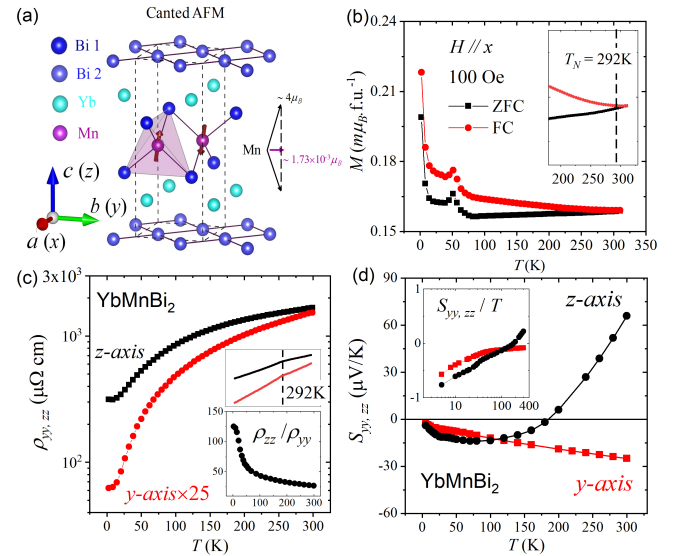


FIG. 1. **The basic properties of YbMnBi₂.** (a) The crystal structure of YbMnBi₂ with two sets of Bi: one kind of Bi is bonded to four Mn atoms while another forms a 2D intercalation network. The spin of Mn cants in the xy plane. (b) Temperature dependence of magnetization M in the xy plane ($H // xy$). (c) Temperature dependence of longitudinal resistivity ρ_{yy} (Red circles) and ρ_{zz} (Black squares). (d) Temperature dependence of Seebeck coefficients S_{yy} (Red squares) and S_{zz} (Black circles).

law breaks down, the Bridgman relation, a consequence of Onsager reciprocity [6], holds.

Here, we report on a careful study of YbMnBi₂ with the aim of quantifying the $zy(cb)$ and $yz(bc)$ components of electric and thermoelectric conductivity tensors. We find that the Hall response obeys Onsager's reciprocal relation. That is: $\rho_{zy}(H) = \rho_{yz}(-H)$ and $\sigma_{zy}(H) = \sigma_{yz}(-H)$. Onsager's reciprocal relations are also veri-

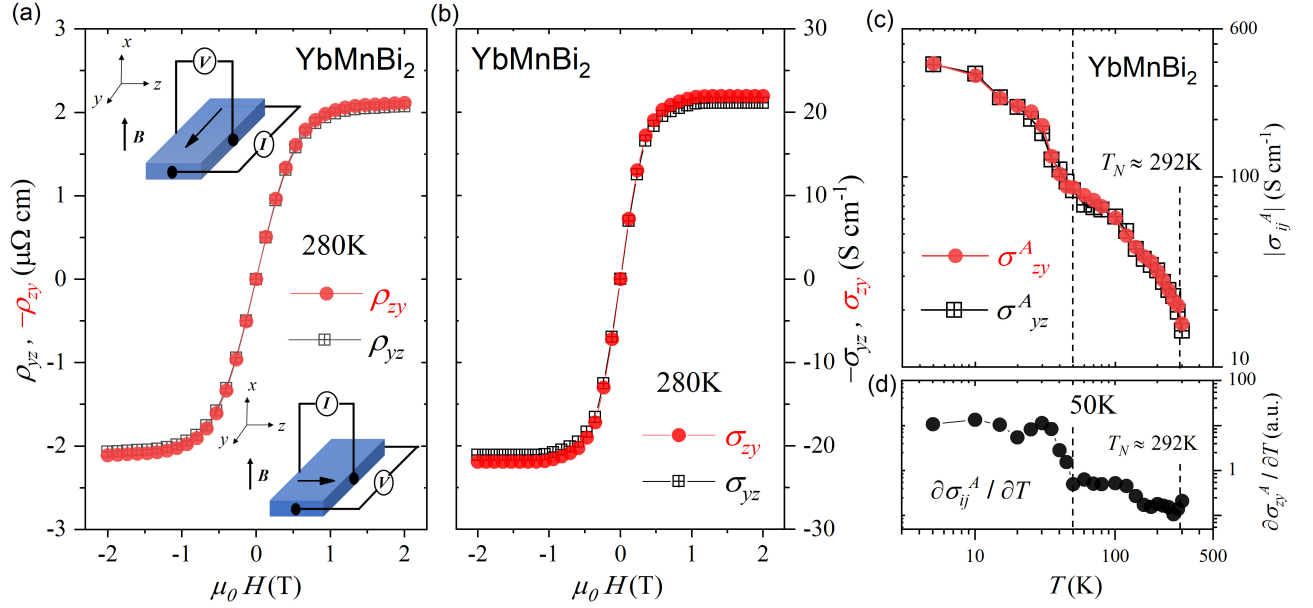


FIG. 2. **Transverse electrical transport.** (a) The setup for measuring Hall signals in the zy and yz configurations. The Hall resistivity is identical, $\rho_{zy} = \rho_{yz}$. (b) The AHC σ_{zy} (σ_{yz}) at 280 K. The Hall conductivity is also identical, $\sigma_{zy} = \sigma_{yz}$. (c) The temperature dependence of anomalous Hall conductivity shows that Onsager's reciprocal is true in the whole temperature range. It exhibits turning an anomaly around 50 K, concomitant with an anomaly in magnetization. (d) The temperature derivative of σ_{ij}^A/T , which shows a kink around 50 K.

fied for the Nernst response: $\alpha_{zy}(H) = \alpha_{yz}(-H)$. On the other hand, and as expected, in the case of Nernst thermopower: $S_{zy}(H) \neq S_{yz}(-H)$. We also examine the temperature dependence of the anomalous transverse thermoelectric response $\alpha_{ij}^A/\sigma_{ij}^A$ ratio[18] and find that this ratio attains a record value of $\approx 2.9k_B/e$ in this system.

Fig.1(b) shows the temperature dependence of M/H observed under $H = 100$ Oe. The Néel temperature T_N is ~ 292 K [1, 10] revealed by a separation point between the field cooling (FC) and the zero field cooling (ZFC), which agrees with previous reports ~ 290 K [1, 9, 11]. At $T \approx 50$ K, we detect for both orientations of temperature sweep, an anomaly not detected before. It indicates a change in the spin canting orientation below and above this temperature.

As illustrated in Fig.1(c), resistivity is metallic and anisotropic. Both ρ_{yy} and ρ_{zz} exhibit a small kink near the Néel temperature. The resistivity anisotropy is ≈ 25 at room temperature and constantly amplifies with cooling, becoming ≈ 125 at low temperature (See the inset of the Fig.1(c)). This indicates that not only the Fermi velocity is anisotropic, but also the relative weight of different carriers and/or scattering mechanisms changes with cooling.

The Seebeck coefficient is also anisotropic as shown in Fig.1(d). S_{yy} is monotonic with temperature. In contrast, S_{zz} is non-monotonic with a peak around 70K and a sign change above 180K. This indicates that S_{zz} has two components with different signs and different variations with temperature. Note that thermopower becomes

isotropic at low temperatures which is expected when it is mostly set by the Fermi energy in the zero temperature regime, as seen in other anisotropic metals[8, 19].

Given the large anisotropy between in-plane, ρ_{yy} , and out-of-plane, ρ_{zz} , resistivity, seen in Fig.1(c), one may wonder about the fate of Onsager's reciprocal relation in the Hall response. As shown in Fig.2(a), it holds. The Hall resistivity, when the magnetic field is along the x -axis is identical when it is measured in the $zy(yz)$ configuration. Here $zy(yz)$ corresponds to a current applied parallel to the $y(z)$ axis and a Hall voltage detected in the $z(y)$ direction. Thus: $\rho_{zy}(H) = \rho_{yz}(-H)$. The field sweep reveals a jump representative of the anomalous Hall effect [13, 16, 20–23]. The Hall conductivity is calculated using $\sigma_{ij} \approx \frac{-\rho_{ij}}{\rho_{ii}\rho_{jj}}$ in Fig.2(b). As shown in Fig.2(c), the two configurations yield identical values for anomalous Hall conductivity (AHC): $\sigma_{zy}^A(H) = \sigma_{yz}^A(-H)$. This equality holds for the whole temperature range (Fig.2(c)).

Thus, Onsager's reciprocal relation is strictly satisfied for Hall resistivity and Hall conductivity, in the presence of a very anisotropic Fermi surface, a magnetic order and a temperature-dependent anisotropy. The origin of the observation reported in ref.[1] is yet to be understood. As discussed in the details in Supplementary Note 3, it might be caused by the oxidation of the samples between two sets of measurements.

Hall conductivities exhibit anomalies around 50K (Fig.2(c)), consistent with the anomaly seen in the magnetization data shown in Fig.1(b). To further illustrate this point, we took the derivative of σ_{ij}^A/T , as depicted

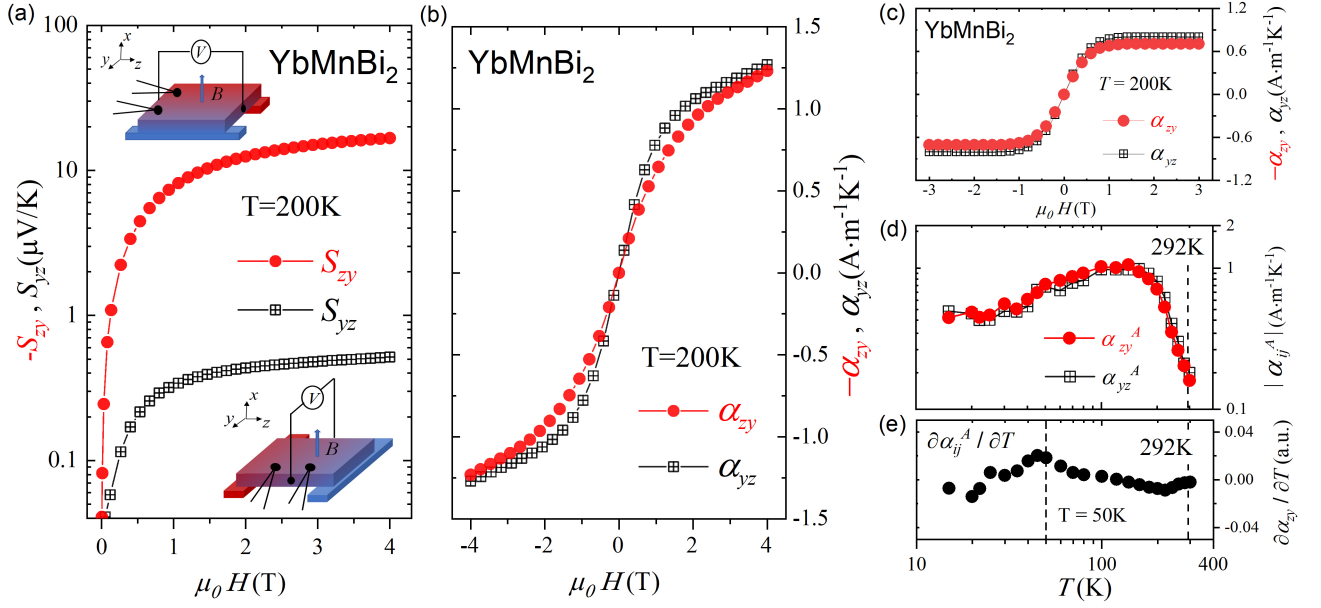


FIG. 3. **Transverse thermoelectric transport.** (a) The setup for measuring Nernst signals in the zy and yz configurations. The transverse thermopower shows an extreme anisotropy in both reciprocal configurations. (b) The anomalous Nernst conductivity is calculated. Its magnitude for the two configurations is identical within experimental error shown the established Onsager's reciprocal relation. (c) The anomalous Nernst conductivity (ANC) α_{zy} (α_{yz}) at 200K. (d) The temperature dependence of ANC shows that Onsager's reciprocal is true in the whole temperature range. It also exhibits a kink around 50K. (e) The temperature derivative of α_{ij}^A/T , which shows a kink around 50K.

in Fig.2(d) and identified a distinct anomaly occurring at 50K. The longitudinal transport does not show any anomaly at 50 K (Fig.1(c)). Therefore, what happens at this temperature concerns the orientation of spins. The Fermi surface or other electronic charge-related properties are not visibly affected.

Let us now examine the relevance of Onsager's reciprocity to the thermoelectric transport. In contrast to its electrical counterpart, the anomalous Nernst effect is driven by a statistical force [24, 25] and the issue deserves to be addressed by the experiment. In Fig.3(a) shows the results of Nernst experiment for two configurations. In the absence of charge current, when a temperature gradient ∇T , is applied, along the y (z) axis, it gives rise to a voltage along the z (y) orientation. Thus, one can compares the responses for zy and yz configurations. As shown in Fig.3(a), $S_{zy} \neq S_{yz}$. At 1 T, the anisotropy is as large as 24. Since S_{ij} is *not* a true Onsager coefficient, this is not a surprising result. On the other hand, α , the thermoelectric conductivity tensor, is an Onsager coefficient which links a force (either the temperature gradient or the electric field) to a flux (the charge density current or the heat density current). The Nernst conductivity is the off-diagonal component of this Onsager tensor: $\alpha_{ij} = S_{ij}\sigma_{ii} + S_{jj}\sigma_{ij}$. It is shown in Fig.3(b). One can see that $\alpha_{zy} = -\alpha_{yz}$ and they both show a jump during the field sweep near zero magnetic field as observed in numerous magnets [1, 13, 16, 18, 26–28], shown in Fig.3(c). Its magnitude for the two configurations is identical within experimental uncertainty: $\alpha_{zy}^A(H) = \alpha_{yz}^A(-H)$. We found that this equality holds

for the whole temperature range (Fig.3(d)).

Onsager's reciprocal relations lead to the following (The details in Supplementary Note 6):

$$\frac{S_{ij}}{S_{ji}} \approx -\frac{\sigma_{jj}}{\sigma_{ii}}. \quad (1)$$

As in the case of the anomalous Hall effect, there is a kink in S_{ij}^A and α_{ij}^A (Fig.3(d) and Supplementary Note 4), near the temperature at which there is an anomaly in magnetization. A more visible anomaly can be seen in the temperature derivative of α_{ij}^A as presented in Figure 3(e). The Seebeck coefficient does not show any anomaly at 50K (Fig.1(d)). This further suggests that what occurs at 50K is a spin-related and not a charge-related phenomenon.

Since Onsager's reciprocity is found to hold in the whole temperature range, let us demonstrate that this implies its validity irrespective of the origin of the anomalous transverse coefficients. Fig.4(a) shows how the amplitude of the anomalous Hall conductivity for the yz configuration varies as a function of longitudinal conductivity as the sample is cooled. Two regions, I and II can be distinguished in this plot. In region I, corresponding to high temperature, above the anomaly in magnetization, σ_{zy}^A increases with increasing σ_{yy} and then saturates to plateau near 50 K. This flat AHC ($\sigma_H^A = (\sigma)^0 = \text{constant}$) is concomitant with the maximum of magnetization at 50K and can be considered as intrinsic AHC [18, 20, 21, 29–31]. As the temperature further decreases and one enters region II, the magnetization increases to

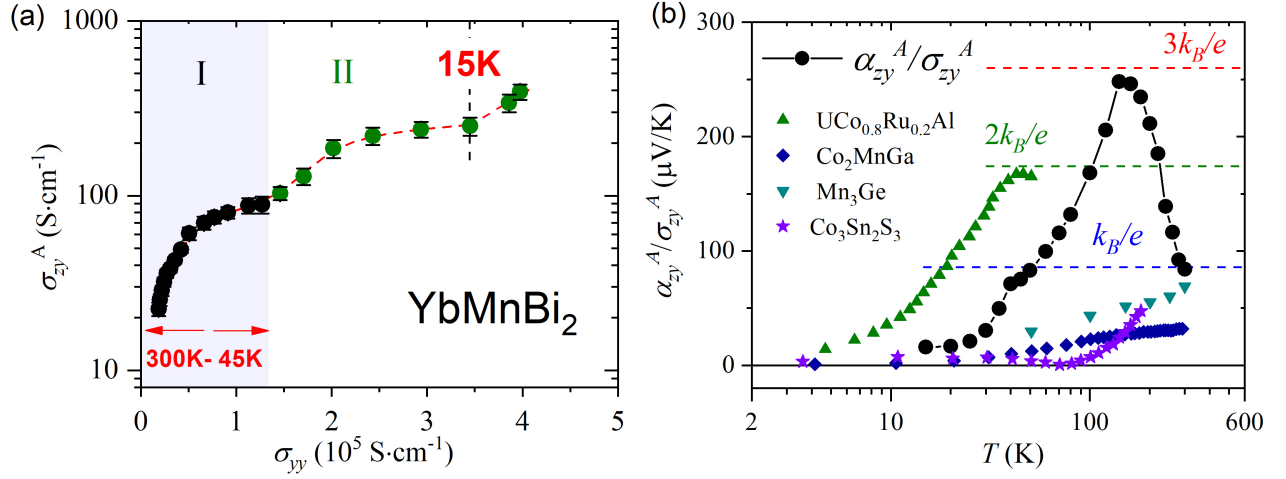


FIG. 4. **Scaling relation of the anomalous Hall conductivity.** The longitudinal conductivity (a) σ_{yy} for YbMnBi₂ lines within the good-metal regime, and there is a crossover behavior to the skew scattering region in the lower temperature, suggesting the Skew scattering will dominate the transverse transport. The flat AHC ($\sigma_H^A = (\sigma)^0 = \text{constant}$) is concomitant with the maximum of magnetization at 50 K, indicating the possible role played by an extrinsic mechanism below this temperature. (b) The α_{zy}/σ_{zy} ratio at different temperatures. Similar to other topological magnets, it approaches 86 $\mu\text{V/K}$ at room temperature, but there is a peak as large as 250 $\mu\text{V/K}$ at 140 K.

a turning point at 15 K, and the AHC also saturates near the same temperature, representing a second value for intrinsic. Between 50 K and 15 K, there is an interval where σ_{zy}^A is an increasing function of σ_{yy} . Here, one may invoke a potentially dominant [32] extrinsic (skew scattering or side jump) mechanism of AHE [20, 31, 33]. On the other hand, the change in the in-plane ferromagnetic component at 50 K affects the intrinsic Berry-curvature. Density functional theory [34] finds that the number of the Weyl node pairs will increase with increasing canted angle. A transformation of the intrinsic Berry curvature at 50 K would explain the observation of two saturated AHC amplitudes around 50 K and 15 K.

Given the presence of both intrinsic and extrinsic components in AHE and the equality between off-diagonal components of AHC and ANC in the whole temperature range, we can conclude that Onsager's reciprocity is relevant to anomalous transverse response regardless of the details of their microscopic origin.

Let us now turn our attention to the relative amplitude of σ_{ij}^A and α_{ij}^A . Xu et al.[18] found that the ratio of $\alpha_{ij}^A/\sigma_{ij}^A$ approaches the ratio of natural units $k_B/e = 86 \mu\text{V/K}$ at room temperature in many topological magnets. The temperature dependence of $\alpha_{ij}^A/\sigma_{ij}^A$ ratio is a monotonic function of temperature and approaches k_B/e near the ordering temperature [29, 30, 35, 36]. In contrast, as shown in Fig.4(b), we find that in YbMnBi₂, the temperature dependence of this ratio is non-monotonic and attains a value as large as $2.9 k_B/e$ at 160K.

In the intrinsic picture, this ratio depends on the way the Berry curvature affects the flow of entropy and the flow of charge [18, 35]. Roughly, the ratio is set by $\frac{k_B}{e} \frac{\langle \lambda_F^2 \rangle}{\langle \Lambda^2 \rangle}$ [18], where $\langle \lambda_F^2 \rangle$ and $\langle \Lambda^2 \rangle$ are the square of the Fermi and the thermal wavelengths averaged over the whole

Fermi surface [18]. As the system is warmed up, the $\alpha_{ij}^A/\sigma_{ij}^A$ ratio monotonically increases and tends towards $\sim \frac{k_B}{e}$ when λ_F and Λ become comparable. A number of theoretical studies have examined the amplitude of this ratio [37, 38]. Qiang *et al.* [38], by performing a Sommerfeld expansion, found that this ratio becomes $\frac{\alpha_{ij}^{int}}{\sigma_{ij}^{int}} = \left(\frac{\mu}{e} + \frac{\pi^2}{3} \frac{k_B^2 T^2}{e\mu} \right)^{-1} L_0 T$. This expression implies an upper boundary of $\sim 0.77 \frac{k_B}{e}$ (See the Supplementary Note 7). Therefore, our observation calls for an approach beyond a single-band degenerate Fermi system subject to Sommerfeld expansion.

The Fermi surface of YbMnBi₂ is known to consist of multiple electron and hole pockets. According to the most recent set of DFT calculations [1], the largest pockets, are electron-like, and have a Fermi energy in the range of ~ 80 meV [1, 9, 11]. This is confirmed by our SdH results (See the supplement) and consistent with the slope of our isotropic thermopower at low temperatures shown in Fig.1(d). $S_{ii}/T \rightarrow 0.6 \mu\text{V/K}^2$ implies a Fermi energy of ~ 50 meV. Since this is the largest energy scale of the system, the Fermi energy of other pockets (and in particular the smaller hole pockets) should be significantly smaller than this and at 150 K, at least one set of hole pockets are non-degenerate.

There is no available theory of intrinsic anomalous Hall effect in presence of non-degenerate electrons. Nevertheless, let us note that non-degenerate electron has more entropy than a degenerate electron ($3k_B$ vs. $2\ln 2 k_B$), but the same electric charge. Therefore, it is plausible that the presence of non-degenerate carriers allow a larger $\alpha_{ij}^A/\sigma_{ij}^A$ ratio. Let us also not forget that the k_B/e boundary may not hold in the presence of multiple bands or when AHE is partially extrinsic.

In summary, we measured electrical and thermoelec-

tric transport properties in YbMnBi₂ and found that Onsager's reciprocal relation is robust. Reciprocity holds in the whole temperature range irrespective of the intrinsic or extrinsic origin of the anomalous transverse response. The $\alpha_{ij}^A/\sigma_{ij}^A$ ratio is exceptionally large, possibly as a result of the presence of non-degenerate electrons.

This work was supported by The National Key Research and Development Program of China (Grant No.2022YFA1403500), the National Science Foundation of China (Grant No. 12004123, 51861135104 and

11574097), and the Fundamental Research Funds for the Central Universities (Grant no. 2019kfyXMBZ071). K. B. was supported by the Agence Nationale de la Recherche (ANR-19-CE30-0014-04). X. L. acknowledges the China National Postdoctoral Program for Innovative Talents (Grant No.BX20200143) and the China Postdoctoral Science Foundation (Grant No.2020M682386).

* zengwei.zhu@hust.edu.cn

* kamran.behnia@espci.fr

-
- [1] Y. Pan, C. Le, B. He, S. J. Watzman, M. Yao, J. Gooth, J. P. Heremans, Y. Sun, and C. Felser, Giant anomalous Nernst signal in the antiferromagnet YbMnBi₂, *Nature Materials* **21**, 203 (2022).
 - [2] L. Onsager, Reciprocal relations in irreversible processes. I., *Phys. Rev.* **37**, 405 (1931).
 - [3] L. Onsager, Reciprocal relations in irreversible processes. II., *Phys. Rev.* **38**, 2265 (1931).
 - [4] P. Mazur and S. R. de Groot, Extension of Onsager's theory of reciprocal relations. II, *Phys. Rev.* **94**, 224 (1954).
 - [5] S. R. de Groot and P. Mazur, Extension of Onsager's theory of reciprocal relations. I, *Phys. Rev.* **94**, 218 (1954).
 - [6] H. B. Callen, The application of Onsager's reciprocal relations to thermoelectric, thermomagnetic, and galvanomagnetic effects, *Phys. Rev.* **73**, 1349 (1948).
 - [7] H. B. G. Casimir, On Onsager's principle of microscopic reversibility, *Rev. Mod. Phys.* **17**, 343 (1945).
 - [8] K. Behnia, *Fundamentals of Thermoelectricity* (Oxford University Press, 2015).
 - [9] A. Wang, I. Zaliznyak, W. Ren, L. Wu, D. Graf, V. O. Garlea, J. B. Warren, E. Bozin, Y. Zhu, and C. Petrovic, Magnetotransport study of Dirac fermions in YbMnBi₂ antiferromagnet, *Phys. Rev. B* **94**, 165161 (2016).
 - [10] J.-R. Soh, H. Jacobsen, B. Ouladdiaf, A. Ivanov, A. Piovano, T. Tejsner, Z. Feng, H. Wang, H. Su, Y. Guo, Y. Shi, and A. T. Boothroyd, Magnetic structure and excitations of the topological semimetal YbMnBi₂, *Phys. Rev. B* **100**, 144431 (2019).
 - [11] S. Borisenko, D. Evtushinsky, Q. Gibson, A. Yaresko, K. Koepernik, T. Kim, M. Ali, J. van den Brink, M. Hoesch, A. Fedorov, E. Haubold, Y. Kushnirenko, I. Soldatov, R. Schäfer, and R. J. Cava, Time-reversal symmetry breaking type-II Weyl state in YbMnBi₂, *Nature Communications* **10**, 3424 (2019).
 - [12] C. Le, C. Felser, and Y. Sun, Design strong anomalous Hall effect via spin canting in antiferromagnetic nodal line materials, *Phys. Rev. B* **104**, 125145 (2021).
 - [13] X. Li, L. Xu, L. Ding, J. Wang, M. Shen, X. Lu, Z. Zhu, and K. Behnia, Anomalous Nernst and Righi-Leduc effects in Mn₃Sn: Berry curvature and entropy flow, *Phys. Rev. Lett.* **119**, 056601 (2017).
 - [14] T. Chen, T. Tomita, S. Minami, M. Fu, T. Koretsune, M. Kitatani, I. Muhammad, D. Nishio-Hamane, R. Ishii, F. Ishii, R. Arita, and S. Nakatsuji, Anomalous transport due to Weyl fermions in the chiral antiferromagnets Mn₃X, X = Sn, Ge, *Nature Communications* **12**, 572 (2021).
 - [15] M. Ikhlas, T. Tomita, T. Koretsune, M.-T. Suzuki, D. Nishio-Hamane, R. Arita, Y. Otani, and S. Nakatsuji, Large anomalous nernst effect at room temperature in a chiral antiferromagnet, *Nature Physics* **13**, 1085+ (2017).
 - [16] L. Xu, X. Li, X. Lu, C. Collignon, H. Fu, J. Koo, B. Fauqué, B. Yan, Z. Zhu, and K. Behnia, Finite-temperature violation of the anomalous transverse Wiedemann-Franz law, *Science Advances* **6**, eaaz3522 (2020).
 - [17] C. Wuttke, F. Caglieris, S. Sykora, F. Scaravaggi, A. U. B. Wolter, K. Manna, V. Süß, C. Shekhar, C. Felser, B. Büchner, and C. Hess, Berry curvature unravelled by the anomalous Nernst effect in Mn₃Ge, *Phys. Rev. B* **100**, 085111 (2019).
 - [18] L. Xu, X. Li, L. Ding, T. Chen, A. Sakai, B. Fauqué, S. Nakatsuji, Z. Zhu, and K. Behnia, Anomalous transverse response of Co₂MnGa and universality of the room-temperature $\alpha_{ij}^A/\sigma_{ij}^A$ ratio across topological magnets, *Phys. Rev. B* **101**, 180404 (2020).
 - [19] T. W. Silk, I. Terasaki, T. Fujii, and A. J. Schofield, Out-of-plane thermopower of strongly correlated layered systems: An application to Bi₂(Sr, La)₂CaCu₂O_{8+δ}, *Phys. Rev. B* **79**, 134527 (2009).
 - [20] N. Nagaosa, J. Sinova, S. Onoda, A. H. MacDonald, and N. P. Ong, Anomalous Hall effect, *Rev. Mod. Phys.* **82**, 1539 (2010).
 - [21] A. Sakai, Y. P. Mizuta, A. A. Nugroho, R. Sihombing, T. Koretsune, M.-T. Suzuki, N. Takemori, R. Ishii, D. Nishio-Hamane, R. Arita, P. Goswami, and S. Nakatsuji, Giant anomalous Nernst effect and quantum-critical scaling in a ferromagnetic semimetal, *Nature Physics* **14**, 1119 (2018).
 - [22] S. Nakatsuji, N. Kiyohara, and T. Higo, Large anomalous hall effect in a non-collinear antiferromagnet at room temperature, *Nature* **527**, 212 (2015).
 - [23] Y. Taguchi, Y. Oohara, H. Yoshizawa, N. Nagaosa, and Y. Tokura, Spin chirality, berry phase, and anomalous hall effect in a frustrated ferromagnet, *Science* **291**, 2573 (2001).
 - [24] D. Xiao, Y. Yao, Z. Fang, and Q. Niu, Berry-phase effect in anomalous thermoelectric transport, *Phys. Rev. Lett.* **97**, 026603 (2006).
 - [25] D. Xiao, M.-C. Chang, and Q. Niu, Berry phase effects on electronic properties, *Rev. Mod. Phys.* **82**, 1959 (2010).
 - [26] N. Hanasaki, K. Sano, Y. Onose, T. Ohtsuka, S. Iguchi, I. Kézsmárki, S. Miyasaka, S. Onoda, N. Nagaosa, and Y. Tokura, Anomalous nernst effects in pyrochlore molybdates with spin chirality, *Phys. Rev. Lett.* **100**,

- 106601 (2008).
- [27] T. Miyasato, N. Abe, T. Fujii, A. Asamitsu, S. Onoda, Y. Onose, N. Nagaosa, and Y. Tokura, Crossover behavior of the anomalous hall effect and anomalous nernst effect in itinerant ferromagnets, *Phys. Rev. Lett.* **99**, 086602 (2007).
 - [28] Y. Pu, D. Chiba, F. Matsukura, H. Ohno, and J. Shi, Mott relation for anomalous hall and nernst effects in $\text{Ga}_{1-x}\text{Mn}_x\text{As}$ ferromagnetic semiconductors, *Phys. Rev. Lett.* **101**, 117208 (2008).
 - [29] S. N. Guin, K. Manna, J. Noky, S. J. Watzman, C. Fu, N. Kumar, W. Schnelle, C. Shekhar, Y. Sun, J. Gooth, and C. Felser, Anomalous Nernst effect beyond the magnetization scaling relation in the ferromagnetic Heusler compound Co_2MnGa , *NPG Asia Materials* **11**, 16 (2019).
 - [30] X. Xu, J.-X. Yin, W. Ma, H.-J. Tien, X.-B. Qiang, P. V. S. Reddy, H. Zhou, J. Shen, H.-Z. Lu, T.-R. Chang, Z. Qu, and S. Jia, Topological charge-entropy scaling in kagome Chern magnet TbMn_6Sn_6 , *Nature Communications* **13**, 1197 (2022).
 - [31] S. Onoda, N. Sugimoto, and N. Nagaosa, Intrinsic versus extrinsic anomalous Hall effect in ferromagnets, *Phys. Rev. Lett.* **97**, 126602 (2006).
 - [32] M. Papaj and L. Fu, Enhanced anomalous Nernst effect in disordered Dirac and Weyl materials, *Phys. Rev. B* **103**, 075424 (2021).
 - [33] Y. Tian, L. Ye, and X. Jin, Proper scaling of the anomalous Hall effect, *Phys. Rev. Lett.* **103**, 087206 (2009).
 - [34] X.-S. Ni, C.-Q. Chen, D.-X. Yao, and Y. Hou, Origin of the type-II Weyl state in topological antiferromagnetic YbMnBi_2 , *Phys. Rev. B* **105**, 134406 (2022).
 - [35] L. Ding, J. Koo, L. Xu, X. Li, X. Lu, L. Zhao, Q. Wang, Q. Yin, H. Lei, B. Yan, Z. Zhu, and K. Behnia, Intrinsic anomalous Nernst effect amplified by disorder in a half-metallic semimetal, *Phys. Rev. X* **9**, 041061 (2019).
 - [36] H. Zhang, J. Koo, C. Xu, M. Sretenovic, B. Yan, and X. Ke, Exchange-biased topological transverse thermoelectric effects in a Kagome ferrimagnet, *Nature Communications* **13**, 1091 (2022).
 - [37] Z. Wang, R. Boyack, and K. Levin, Heat-bath approach to anomalous thermal transport: Effects of inelastic scattering, *Phys. Rev. B* **105**, 134302 (2022).
 - [38] X.-B. Qiang, Z. Z. Du, H.-Z. Lu, and X. C. Xie, Topological and disorder corrections to the transverse Wiedemann-Franz law and Mott relation in kagome magnets and Dirac materials, *Phys. Rev. B* **107**, L161302 (2023).
 - [39] N. Ashcroft and N. Mermin, *Solid State Physics* (Cengage Learning, 2011).

Supplementary information for “Verification of Onsager reciprocal relation between anomalous transverse coefficients of an anisotropic antiferromagnet”

Supplementary Note 1. Single-crystal preparation and methods

The YbMnBi₂ single crystals were synthesized using a self-flux method with the stoichiometric mixture of Yb, Mn, and Bi elements with an elemental ratio of Yb:Mn:Bi of 1:1:6. The starting materials were put into a small alumina crucible and sealed in a quartz tube in Argon gas atmosphere. The tube was then heated to 1050 °C for 2 days, followed by a subsequently cooling down to 400 °C at a rate of 2 °C h⁻¹. The plate-like single crystals as large as a few millimeters can be obtained.

The samples discussed in the main text were also examined by the energy dispersive spectroscopy (EDS) to determine their compositions. The results are listed in Fig. S1 and table S1.

The experimental methods were the same as the previous reports[13, 16, 18, 35].

TABLE S1. Elemental ratios in YbMnBi₂ samples from EDS, showing a consistent chemical composition result.

Spectrum Label	Yb (Atomic %)	Mn (Atomic %)	Bi (Atomic %)
Map Data 1	25.36	25.16	49.48
Spectrum 1	25.67	24.94	49.39
Spectrum 2	26.06	25.39	48.55
Spectrum 3	25.36	25.15	49.49

Supplementary Note 2. Sign convention of transverse transport measurements

Here we elaborate on the sign convention of transverse transport measurements. For this purpose, Supplementary Fig.S2 shows the schematics of experimental device.

i). ρ_{ii} , σ_{ii} and S_{ii} : for ρ_{ii} , σ_{ii} , the sign is always positive. For S_{ii} , the sign is defined as

$$S_{ii} = -\frac{\Delta V_{ii}}{\Delta T_{ii}} = -\frac{V_2 - V_1}{\Delta T_{ii}}. \quad (S1)$$

ii). Hall effect ρ_{ij} : A the schematic figure is shown in Fig. S2(a). We define $\rho_{ji} = \frac{V_{ij}}{I} = \frac{V_3 - V_2}{I}$, where I is the magnitude of the electric current passing through the sample.

iii). Nernst effect S_{ij} : As shown in Fig. S2(b). We define Nernst coefficient's sign is $S_{ij} = \frac{(V_3 - V_2)/w}{\Delta T_{ii}/l}$.

Supplementary Note 3. longitudinal magnetoresistance and quantum oscillations (SdH)

Fig.S3 displays the magnetoresistance (MR) in y ($I//y$ and $V//y$) and z ($I//z$ and $V//z$) directions. The results indicate anisotropic behaviors, with the MR for ρ_{yy} showing negative magnetoresistivity with increasing temperature, while ρ_{zz} consistently demonstrates positive magnetoresistivity.

Quantum oscillations in magnetoresistivity (SdH) can be observed when the magnetic field is along the z axis (Fig.S4(a) and (b)). From the fast Fourier transform (FFT) background-subtracted oscillating component $\Delta\rho_{xx}$ features frequency $F_\alpha = 125$ T and $F_\beta = 165$ T at 3 K (Fig.S4(c)). From the Onsager relation, $F = (\Phi_0/2\pi^2)A_F$, where Φ_0 is the flux quantum and A_F is the orthogonal cross-sectional area of the Fermi surface. We estimate A_F to be 1.95 nm⁻² and 1.48 nm⁻² corresponding to the measured frequencies of 165 T and 125 T, respectively. The Fermi energies of the two pockets is 102 meV and 62 meV.

Supplementary Note 4. Magnetization measurements

The temperature dependence of the magnetization curves is shown in Fig.S5 (a) and (b) for the field parallel to the x and the z axes. There is a strong anisotropy in the two configurations. As shown in Fig.S5 (c) and (d), magnetization shows a field dependence along the xy plane indicating a canted antiferromagnetic feature of YbMnBi₂.

Supplementary Note 5. Anomalous Hall effect

The Hall resistivity was measured from 300 K to 5 K, as shown in Fig.S6. The Hall conductivity is calculated using $\sigma_{ij} = \frac{-\rho_{ij}}{\rho_{ii}\rho_{jj} + \rho_{ij}\rho_{ji}}$, and is shown in Fig.S7. At each temperature, the Hall conductivity can be empirically expressed as

$$\sigma_{zy} = \sigma_{zy}^A + \sigma_{zy}^T + R_0 B = \sigma_H M + \sigma_{zy}^T + \sigma_0 B. \quad (S2)$$

Here, R_0 and R_H correspond to the normal and anomalous Hall coefficients, respectively. ρ_{zy}^T is the topological Hall effect (THE). For example, at 120 K, the normal Hall effect is linearly fitted and subtracted in Fig.S8 (f). Also, the anomalous and topological Hall signals are shown in Fig.S8 (d) and (e), in which the Hall signals are identical in both reciprocal configurations and remain true in the whole temperature range as shown in Fig.S8 (g), (h), and (i), respectively.

It is worth noting that YbMnBi₂ samples are extremely susceptible to oxidation. In Fig.S9, the Hall resistivity is different at identical temperatures for the same sample if it is stored in a poor vacuum environment for four days.

Supplementary Note 6. Anomalous Nernst effect

The experiment results of the anomalous Nernst effect (ANE) are shown in Fig.S10 and Fig.S12. In the zy configurations, the anomalous Nernst (ANE) is obvious from the 300 K to 10 K; however, the S_{yz} suddenly appears a signal change at the 25 K. Similar to the Hall effect, the Nernst conductivities are contributed with anomalous Nernst conductivity (ANC), α_{ij}^A , topological Nernst conductivity (TNC), α_{ij}^T , and normal Nernst conductivity (NNC), α_0 , which can be expressed as

$$\alpha_{ij} = \alpha_{ij}^A + \alpha_{ij}^T + \alpha_0 = \alpha_H M + \alpha_{ij}^T + \alpha_0. \quad (S3)$$

The value of ANC is summarized in Fig.S12 (f), which shows $\alpha_{zy}^A = \alpha_{yz}^A$. As discussed in the main text, the transverse entropy flux derived by a statistical force is linked to the kinetic coefficient known as Peltier's coefficient α_{ij} rather than the thermopower S_{ij} . The topological and normal Nernst conductivity also can establish Onsager's reciprocal relation in the whole temperature range shown in Fig.S12 (g) and (h).

The Nernst conductivity is the off-diagonal component of this Onsager tensor: $\alpha_{ij} = S_{ij}\sigma_{ii} + S_{jj}\sigma_{ij}$. By utilizing Onsager's reciprocal relation, we can obtain $\alpha_{zy} = -\alpha_{yz}$ in the same field. We can obtain that

$$\sigma_{yy}S_{yz} + \sigma_{yz}S_{zz} = -\sigma_{zz}S_{zy} - \sigma_{zy}S_{yy}. \quad (S4)$$

By utilizing Onsager's reciprocal relation again for Hall conductivity, $\sigma_{zy} = -\sigma_{yz}$, the equation(S4) can be rewritten as

$$S_{yz} = -\frac{\sigma_{zz}}{\sigma_{yy}}S_{zy} - \frac{\sigma_{zy}}{\sigma_{yy}}(S_{yy} - S_{zz}). \quad (S5)$$

Here we ignore the small amount $\frac{\sigma_{zy}}{\sigma_{yy}}(S_{yy} - S_{zz})$ to obtain the following conclusion

$$\frac{S_{ij}}{S_{ji}} \approx -\frac{\sigma_{jj}}{\sigma_{ii}}, \quad (S6)$$

which means that the value of Nernst thermopower will be apportioned by the mobility μ_{ii} , giving rise to an enhanced thermopower in one of the configurations for an anisotropic system. Note that thermopower becomes isotropic at low temperatures which results in the equation(S6) more accurate.

Supplementary Note 7. The $\alpha_{ij}^A/\sigma_{ij}^A$ ratio

Qiang *et al.* have recently proposed this expression for the ratio of the anomalous Nernst to anomalous Hall conductivities in the intrinsic picture[38]:

$$\frac{\alpha_{ij}^{int}}{\sigma_{ij}^{int}} = \left(\frac{\mu}{e} + \frac{\pi^2}{3} \frac{k_B^2 T^2}{e\mu} \right)^{-1} L_0 T. \quad (S7)$$

This expression was obtained using a Sommerfeld ex-

pansion, which is valid only deep in the degenerate regime (when $\mu \ll k_B T$) [39]. Let us write this expression in an explicit way:

$$\frac{\alpha_{ij}^{int}}{\sigma_{ij}^{int}} = \left(\frac{\mu}{e} + \frac{\pi^2}{3} \frac{k_B^2 T^2}{e\mu} \right)^{-1} \frac{\pi^2}{3} \frac{k_B^2}{e^2} T = \frac{k_B}{e} \left(\frac{\pi^2}{3} \frac{\mu}{k_B T} + \frac{k_B T}{\mu} \right)^{-1} \quad (S8)$$

If $\frac{k_B T}{\mu} = 1$, then $\frac{\alpha_{ij}^{int}}{\sigma_{ij}^{int}} = 0.77 k_B/e$. However, Sommerfeld expansion is only allowed when $\frac{k_B T}{\mu} \ll 1$. This indicates that to explain our observation one should invoke multiple bands and possibly the presence of non-degenerate carriers.

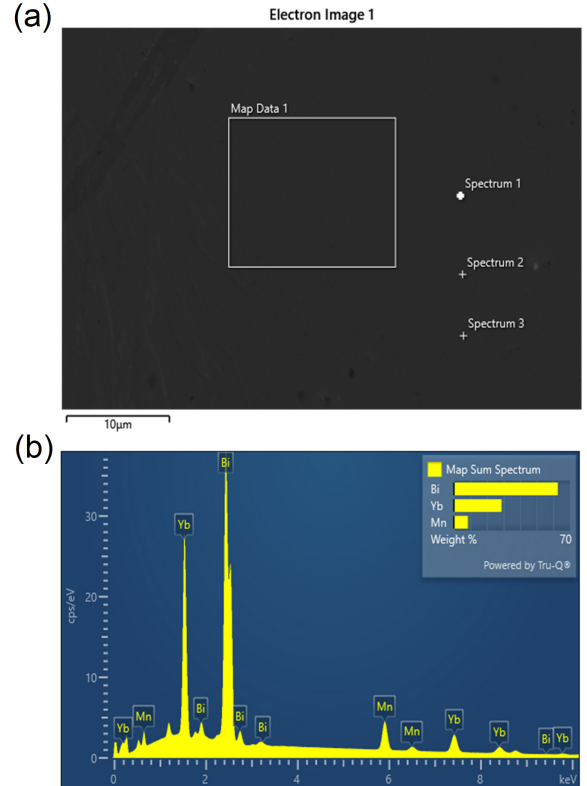


FIG. S1. (a) Scanning electron microscope (SEM) images for the samples discussed in the main text. (b) Energy dispersive spectroscopy (EDS) spectrum of map data of the samples.

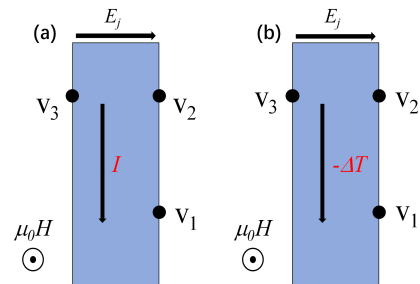


FIG. S2. Sign definition for Hall (a) and Nernst signals (b) in our experimental setup.

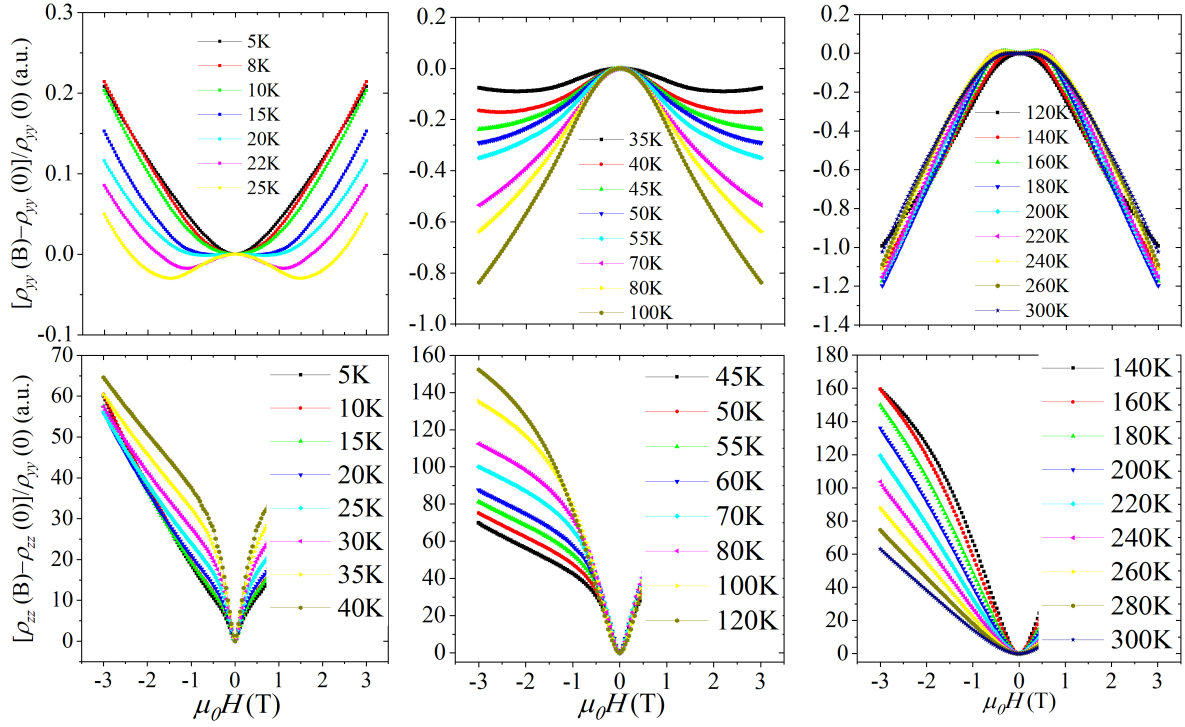


FIG. S3. The field dependence of resistivity at various temperatures for the two configurations. (Upper panels). ρ_{yy} ($B//x$, with the current along the y axis, $I//y$). Negative magnetoresistance is observed when the temperature is above 15 K. (Lower panels). When the applied current is along the z axis and $B//x$, magnetoresistance ρ_{zz} is always positive.

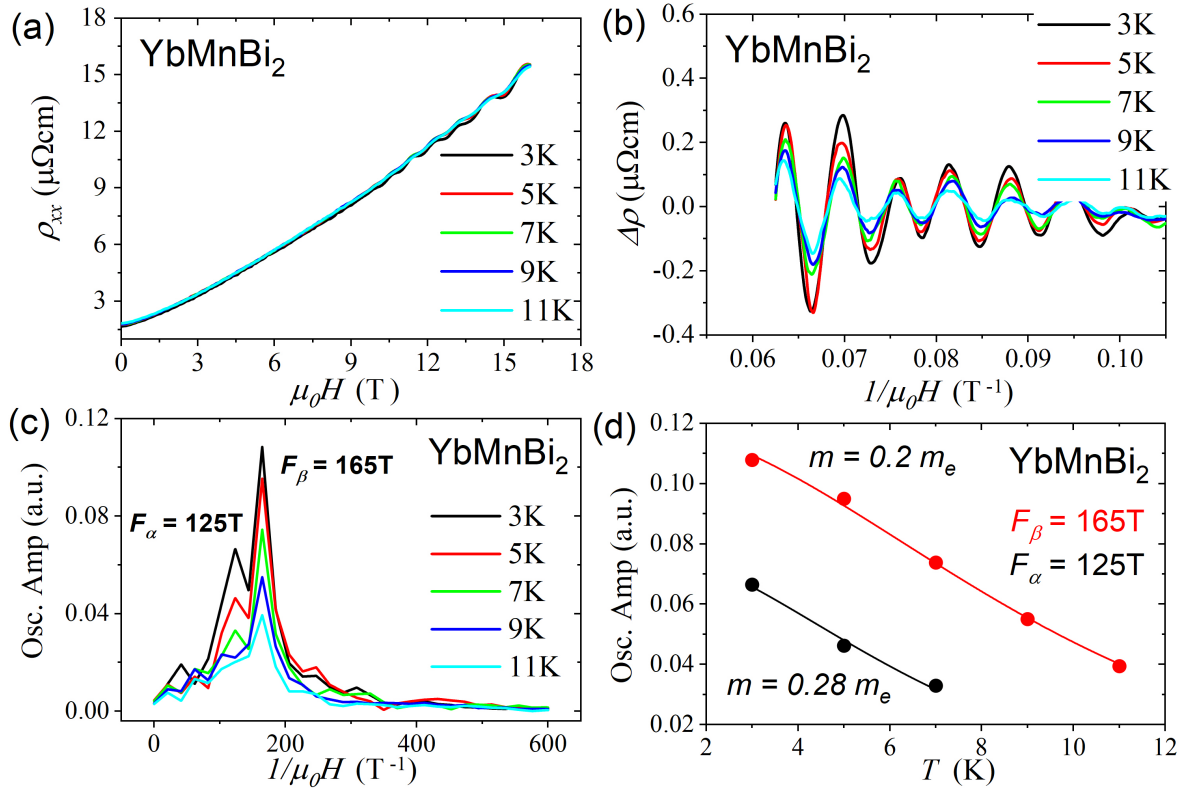


FIG. S4. (a) The field dependence of resistivity, ρ_{xx} ($B//z$, when the current is along the x axial, $I//x$). (b) Oscillations after the background subtraction. (c) The FFT spectrum of the oscillations. (d) The temperature dependence of the oscillating amplitude of magnetoresistivity. The solid line is the fitting curve with the Lifshitz-Kosevich model.

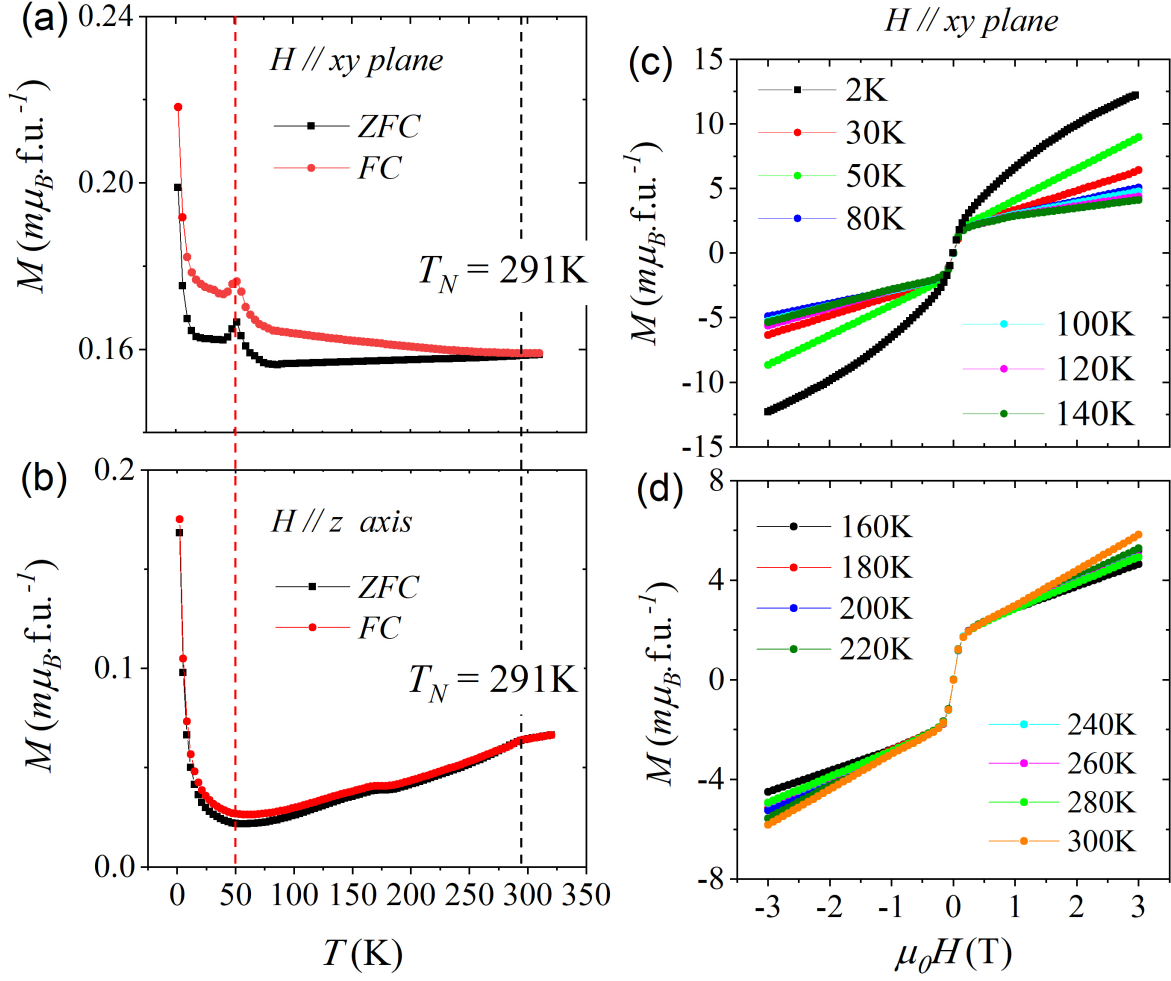


FIG. S5. (a),(b) Temperature dependence of Zero-field-cooled (ZFC) magnetization and field-cooled (FC) magnetization M in the in-plane ($H // xy$) and out-plane ($H // z$) with 100 Oe. At 50K, the response is anisotropic. When the field is parallel to the xy plane, there is a peak, but is absent in the perpendicular orientation ($H // z$). (c), (d) The field dependence of the magnetization at various temperatures when the field is parallel to the xy plane.

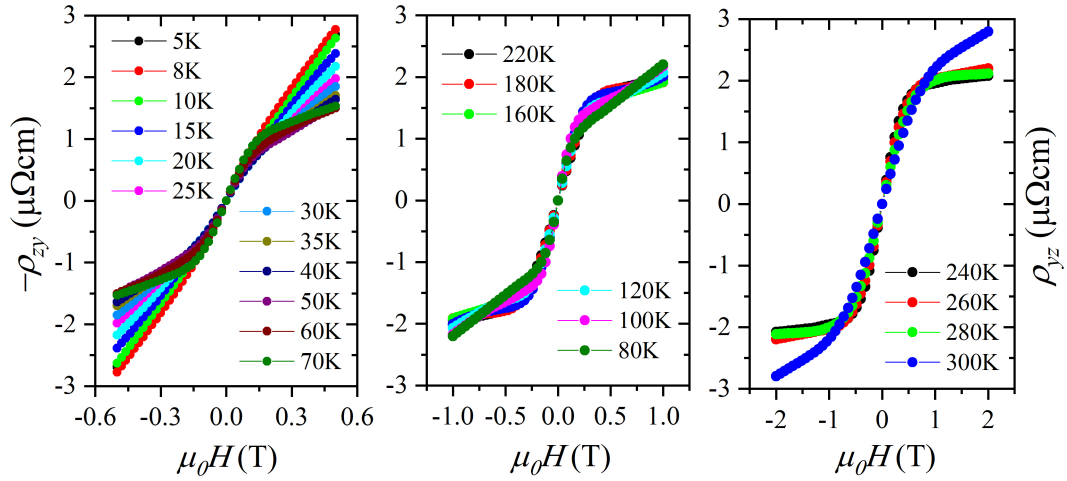


FIG. S6. The magnetic field dependence of the Hall effect at different temperatures. For zy and yz configurations, the Hall resistivity is identical: $\rho_{zy}(B) = \rho_{yz}(-B)$.

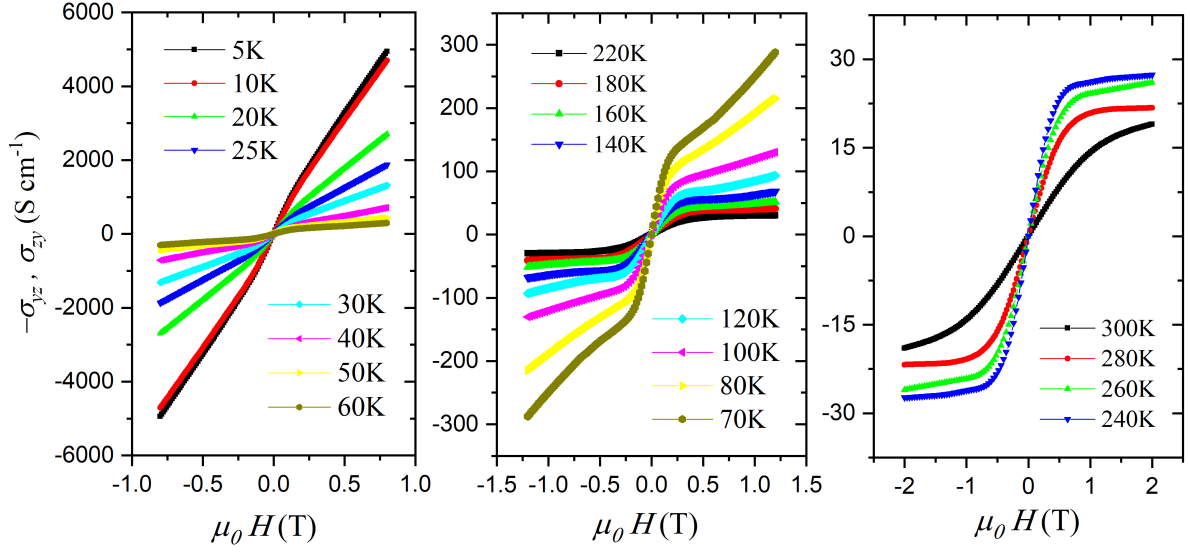


FIG. S7. The field dependence of Hall conductivity at different temperatures. The Hall conductivity is identical, in the two configurations : $\sigma_{zy}(B) = \sigma_{yz}(-B)$.

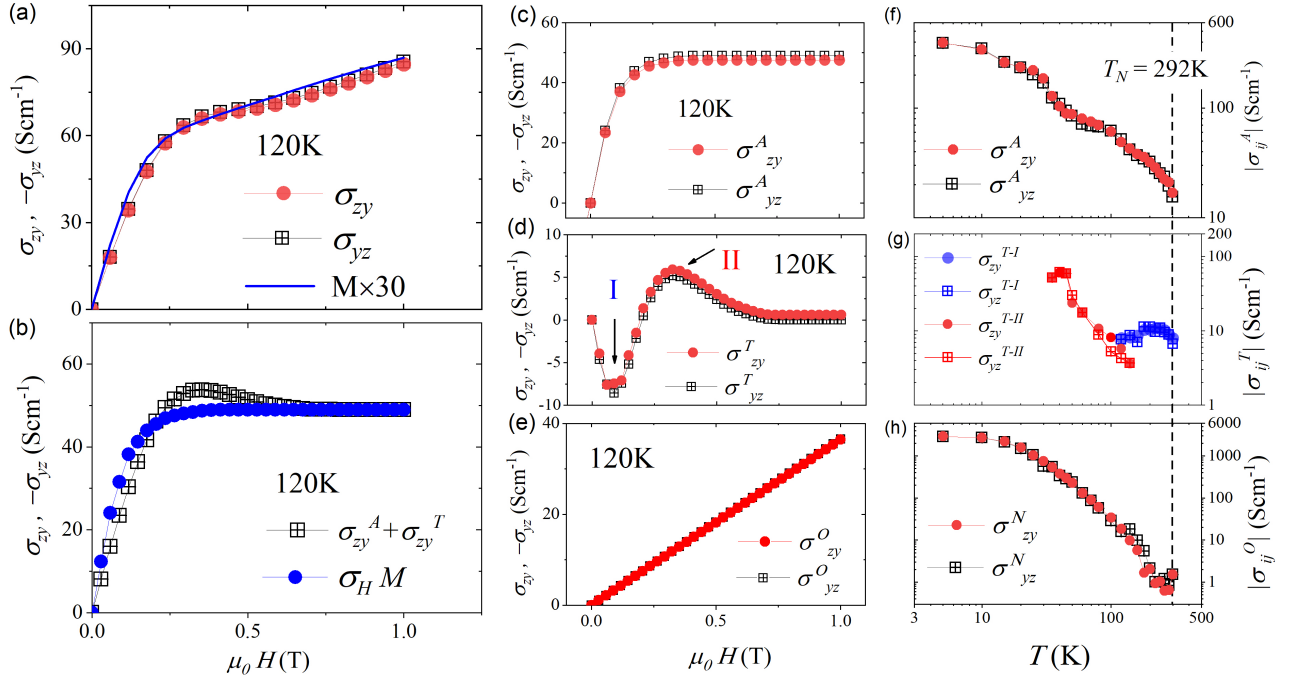


FIG. S8. Hall conductivity analyzed using equation S2. (a) Hall conductivity in the zy and yz configuration compared with the magnetization at the 120 K. Note the peak around 0.3 T. (b) The Hall conductivity minus with its ordinary component subtracted compared with the product of magnetization and the ordinary Hall effect. The maximum near 0.3 T is attributed to the topological Hall effect. The anomalous, topological, and ordinary Hall conductivities are displayed in (c), (d), and (e). The temperature dependence of these three components are shown in (f), (g), and (h).

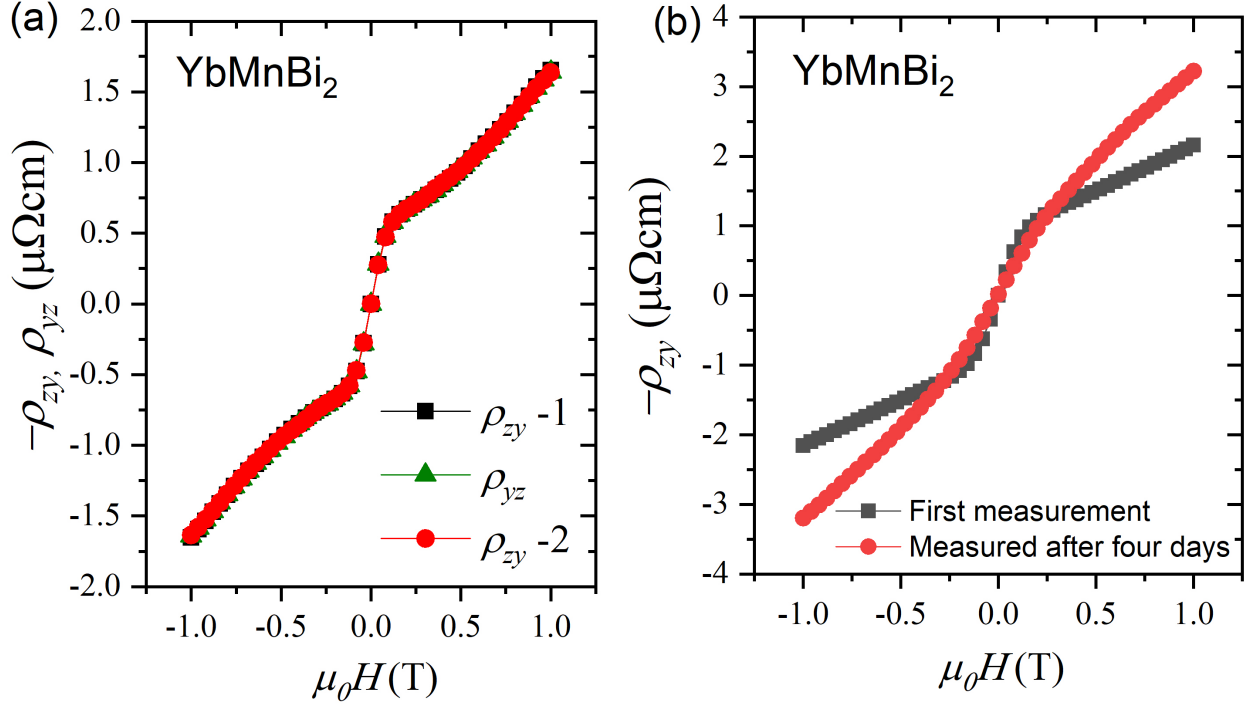


FIG. S9. Oxidation of YbMnBi₂. (a) The properties do not change when the sample undergoes a circulation measurement ($\rho_{zy} \rightarrow \rho_{yz} \rightarrow \rho_{zy}$) under high vacuum. (b) Hall resistivity is different at identical temperatures in the same sample when it is stored in a poor vacuum environment for four days.

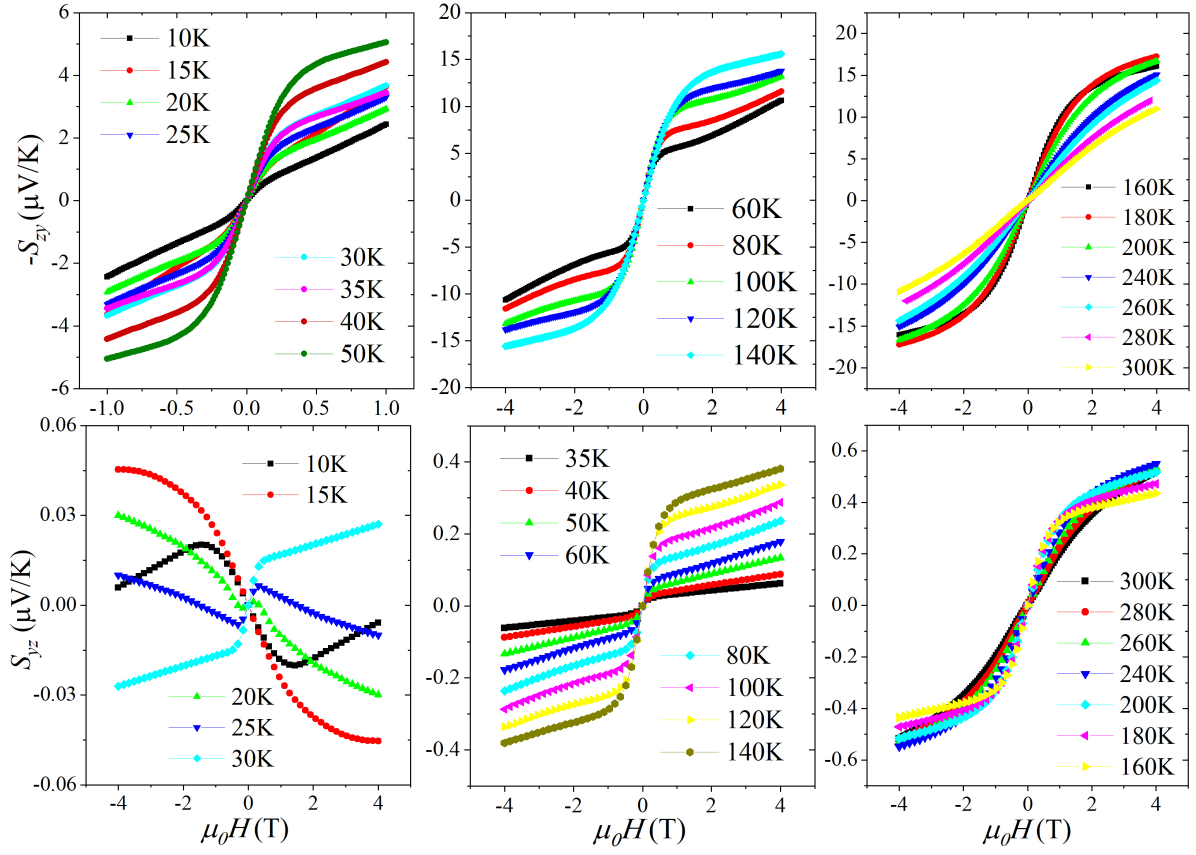


FIG. S10. The magnetic field dependence Nernst effect at different temperatures in zy and yz configurations. In zy and yz configurations, Nernst signal is dramatically different: $\alpha_{zy}(B) \neq \alpha_{yz}(-B)$.

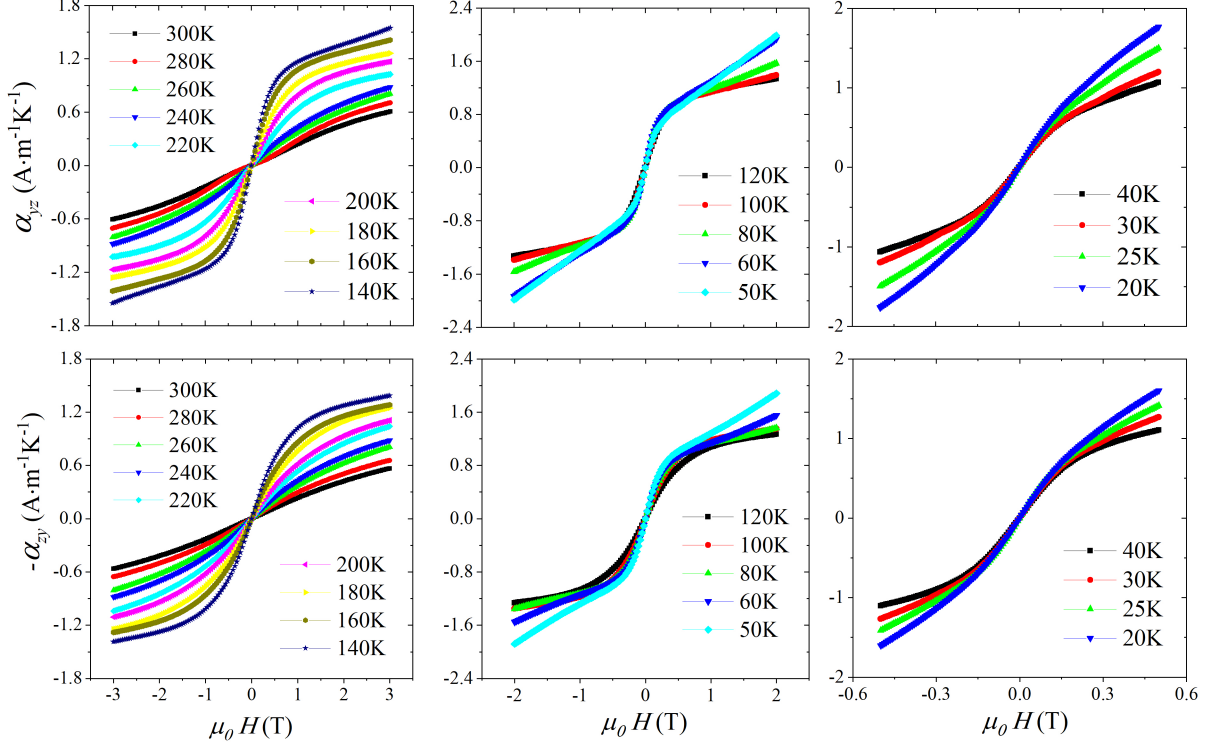


FIG. S11. The field dependence of Nernst conductivity at different temperatures. In zy and yz configurations, Nernst conductivity is identical: $\alpha_{zy}(B) = \alpha_{yz}(-B)$.

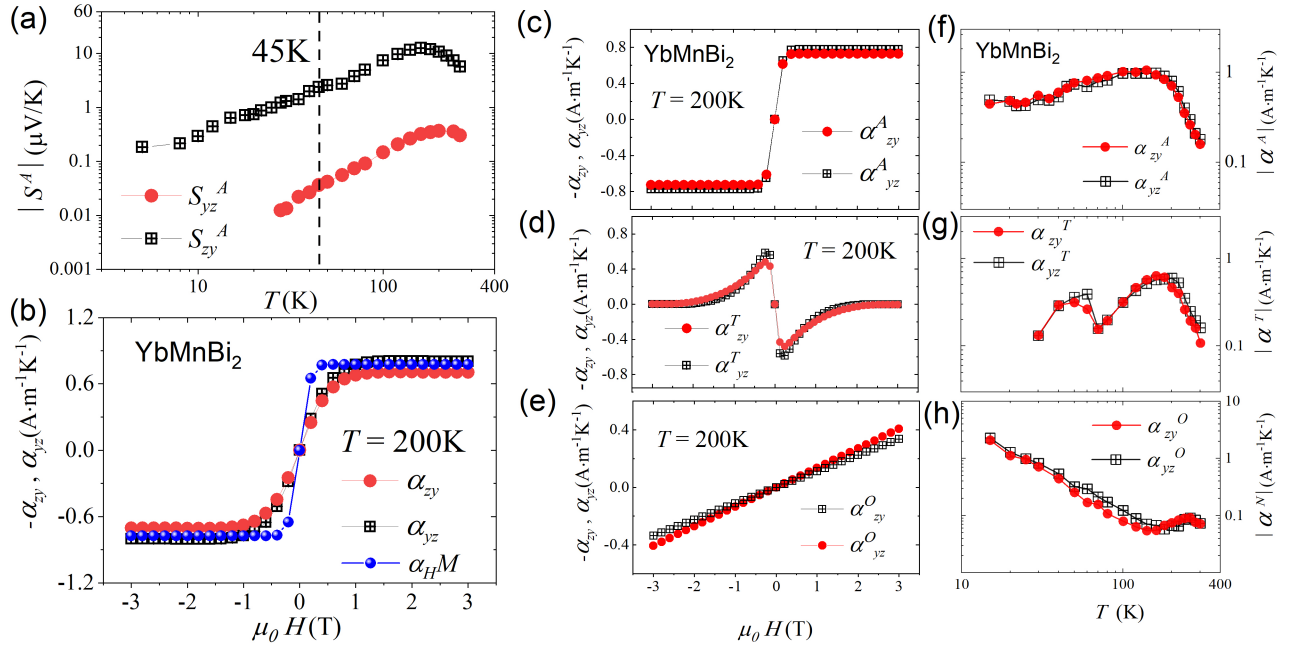


FIG. S12. (a) The anomalous Nernst thermopower in the zy and yz configurations. (b) The Nernst conductivity in the zy and yz configuration compared with the magnetization at 200 K. The anomalous, topological, and ordinary Nernst conductivities are displayed in (c), (d), and (e). The temperature dependence of the three components (anomalous, topological, and ordinary) is shown in (f), (g), and (h).

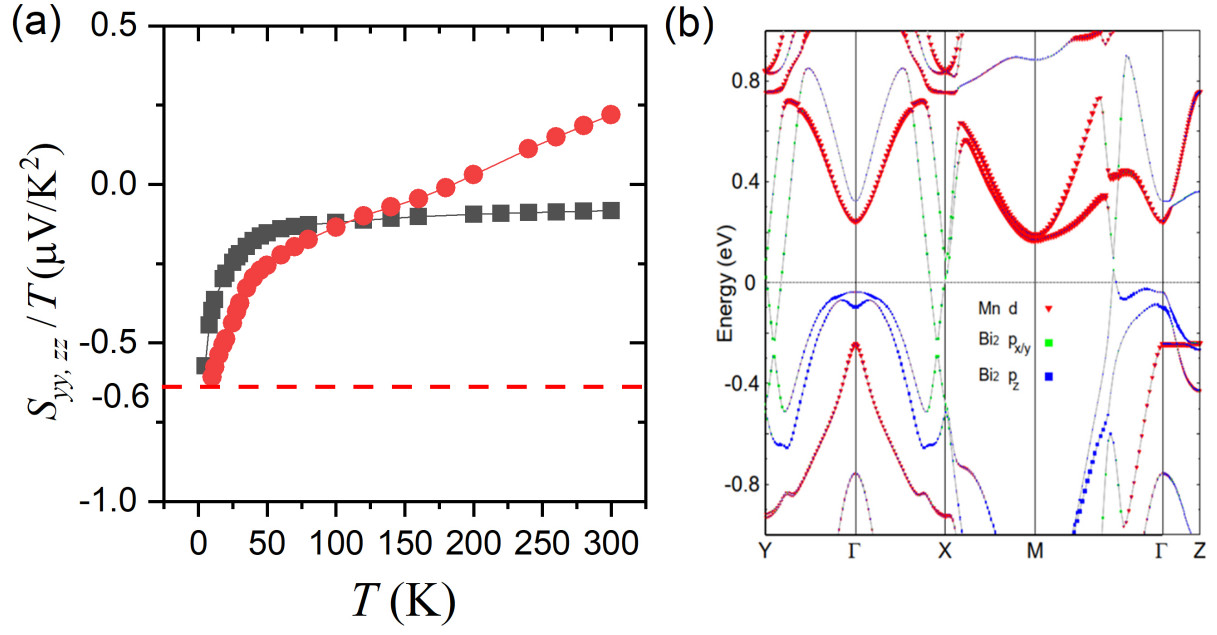


FIG. S13. (a) The temperature dependence of the S_{ii}/T . S_{ii}/T becomes isotropic at low temperatures. Its rough amplitude of $\approx 0.6\mu\text{V}/\text{K}^2$ is consistent with a Fermi energy of 76 meV (b) The Fermi level obtained by DFT calculation[1]. Fermi energy is higher for electrons pockets than for hole pockets.